euspen's 25th International Conference & Exhibition, Zaragoza, ES, June 2025
www.euspen.eu

Design of an aerostatic spindle with a tapered journal bearing preloaded with a planar thrust bearing

Luke Harding[1], Mikael Miettinen[1], Valtteri Vainio[1], Raine Viitala[1]

[1]*Aalto University*

Luke.harding@aalto.fi

Abstract

Porous aerostatic bearings are often implemented in assemblies such as machining spindles and turbo machinery when high rotational speed, low runout, and low wear is desired. Their favourable friction, stiffness, and maintenance characteristics inspired the development of a glass optical fibre guidance spindle using aerostatic bearing technology. Current designs for spindles in optical fibre manufacturing machines include conventional caged ball or roller bearings, which can cause undesirable vibrations resulting in poor quality products, and in some cases, maintenance shutdowns due to fibre breakage.

This study outlines the design, development, and testing of an optical fibre spindle supported by two porous aerostatic bearings: a conical journal bearing and an annular thrust bearing. The measurement setups used to conduct the spindle's balancing procedures, static and dynamic stiffness measurements, and dynamic performance measurements include precision engineering design principles such as compliant mechanisms, capacitive distance measurement, and rotational guidance with aerostatic bearings. Using these setups, the spindle's imbalance was measured at 0.225 gmm at a speed of 6 000 RPM. The static axial stiffness was found to be 8.2 $N\mu m^{-1}$ when loaded with 5 N of axial force. The frictional moment of the aerostatic fibre spindle was found to be 3.7 Nmm under approximately 500 g of radial load at 6 000 RPM, however, the test results suggest contact between the spindle hub and bearings was present. These results show promising characteristics of using an aerostatic spindle and justify further research into the viability of implementing aerostatic bearings in the optical fibre production industry.

Gas lubrication, rotor dynamics, externally pressurized air bearing, tapered bearing, fibre optics

1. Introduction

Aerostatic bearings are key components in modern turbo machines due to their favorable characteristics over conventional roller element bearings at high rotational speeds. When low runout and high long-term performance is needed at elevated speeds, aerostatic bearings are desirable options for supporting rotating assemblies. Spindles found in precision-machining devices almost exclusively use porous aerostatic bearings coupled with air turbines to achieve tooling speeds in excess of 100 000 RPM [1, 2, 3]. These bearings support the spindle in an almost frictionless manner while remaining adequately stiff. Designs for high-precision machining spindles usually include two families of porous aerostatic bearings: journal bearings and planar thrust bearings. Often, two aerostatic journal bearings are combined with one or two aerostatic or conventional thrust bearings to constrain the rotor [4, 5].

A design technique that is uncommon among aerostatic spindles includes supporting a rotating assembly with one tapered journal bearing and one planar thrust bearing. Spindles or turbo machinery with tapered bearings often implement two opposing concial bearings to support the rotating assembly [6]. This study outlines the design and testing of a low-speed spindle system supported by two porous aerostatic bearings: one tapered radial bearing and one annular planar thrust bearing.

The developed spindle targets, but is not limited to, the glass optical fibre production industry. It could provide the industry with an improved system for guiding glass optical fibres in fibre manufacturing machines. A common method of cooling optical fibres after their extrusion stage include guiding the newly-formed fibre through a series of V-grooved pulleys. The fibre is cooled by the surrounding air as it passes through the pulley system. These pulleys are typically supported by rolling-element bearings. Velocity ripples and vibrations induced by inconsistencies in the rolling elements can transfer to the pulley resulting in the potential fracturing of the delicate fibre. Due to the favorable friction and maintenance characteristics of aerostatic bearing systems, porous aerostatic bearings could be used to support the pulleys instead of rolling element bearings.

Provided in this work is the design of the aerostatic spindle, its measured radial and axial stiffnesses, and the bearing system's measured friction moment during operation. The measurement setups include precision engineering concepts such as elastic hinges, capacitive distance sensing, and aerostatic motion guidance.

2. Methods

2.1 Design

The spindle consists of a 316L stainless steel rotor supported by a tapered aerostatic radial bearing and preloaded with an annular aerostatic thrust bearing (Figure 1). The taper ratio of the tapered aerostatic bearing is 0.38. Both bearing surfaces are made from porous graphite and share a single air supply. A banjo bolt ensures the central air supply reaches the thrust bearing and also determines the thrust bearing's preload. This design is manufacturable on a two-axis CNC lathe and only has two critical surfaces: the tapered inner surface of the hub and the hub's planar thrust face. If any small discrepencies in the taper ratio of either part are present, the hub can be worn into

the graphite journal bearing. The graphite will then wear away and match the taper ratio of the stainless steel hub. The hub's thrust face was lapped with a diamond-grit surface plate to mend any surface irregularities produced by the CNC turning process.

The fibre pulley is mounted to the pulley hub with six M4 bolts. Important dynamic and dimensional properties of the fibre pulley were provided by an industry partner. The maximum imbalance of the pulley was 4 mg at a 75 mm radius. The required operating conditions of the spindle are at a speed of 6 000 RPM with 500 g of radial load.

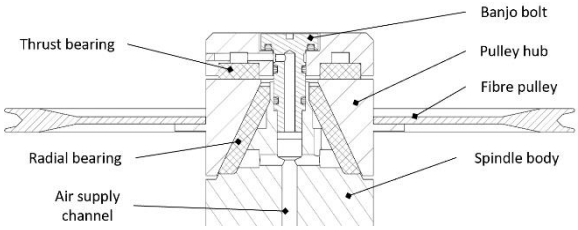

Figure 1. Cross section showing aerostatic spindle internals. The radial and thrust bearing are fed from a single air supply.

2.2. Fibre pulley dynamic balancing

A single-plane balancing setup was constructed to balance the hub and pulley according to the criteria previously provided. The spindle system was mounted in a single-degree-of-freedom fixture that used elastic hinges to constrain any motion produced by imbalance forces to the horizontal plane (Figure 2). The fixture's horizontal motion was observed with a capacitive distance sensor, and the pulley's rotational velocity was measured with a laser tachometer. Using a test mass of 160.0 mg, the pulley was balanced to (3.0 ± 0.1) mg at a 75.0 mm radius and a rotational velocity of 6 048 RPM.

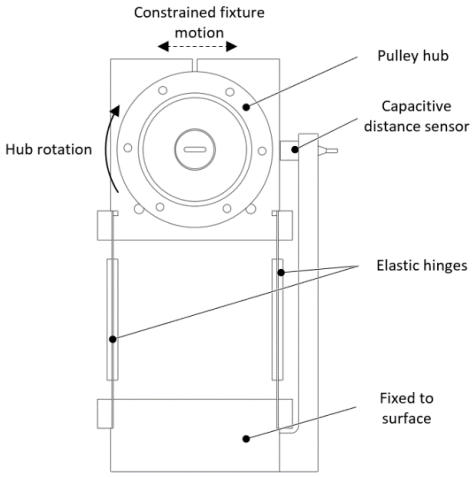

Figure 2. Single plane balancing setup. The fibre pulley is hidden to show the sensor and hinges behind it.

2.3. Static axial stiffness of the radial bearing

In addition to the dynamic balancing setup, a measurement assembly to determine the static axial stiffness of the radial bearing was constructed (Figure 3). Three capacitive distance sensors spaced 120° apart observed the fibre pulley's axial displacement when loaded. The loading hook interacts with the spindle through "sphere and ring" contact. The sphere was indicated at (18 ± 1) µm total runout in relation to the center axis of the spindle with a dial indicator. A thin strip of tape was fixed against the fibre pulley and capacitive sensor mount to lock the angular position of the pulley during the loading trial. The measurement procedure was as follows:

1. Measure an initial displacement reading with only the loading hook and cable attached.
2. Place a 100 g mass on the loading hook cable.
3. Wait 30 s until the loading hook and mass settle.
4. Gather 10 distance readings from each sensor.
5. Unload the mass and repeat steps 2-4 in 100 g increments until 1 000 g is tested.

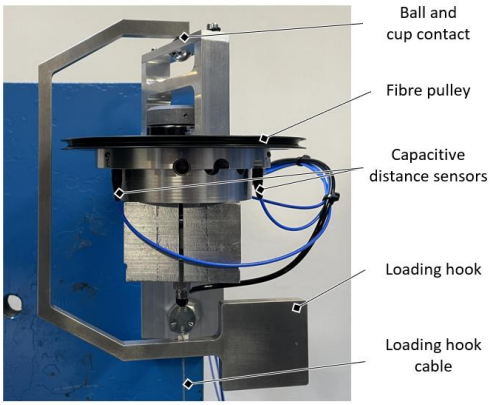

Figure 3. Axial stiffness measurement setup. The spindle is loaded with masses that are hung with a string from a hook, minimizing adverse moment loads.

2.4. Static radial stiffness of the spindle

To supplement the measurement of the spindle's static axial stiffness, a measurement setup to determine its static radial stiffness was constructed. The spindle was fixed parallel to the horizonal plane and loaded with various masses hung from a thin wire contacting the fibre pulley groove (Figure 4). A total of five capacitive distance sensors observed the deflection of the pulley hub during testing. Three sensors, spaced 120° from one another, observed the axial displacement of the hub and two observed the hub's radial displacement. The first radial displacement sensor was mounted 7 mm from the center of the hub, and the second one was mounted 12 mm from the first. The measurement procedure was identical to the static axial stiffness procedure with 1 000 g as the maximum tested mass. A thin piece of tape was again used to lock the pulley's rotation during testing.

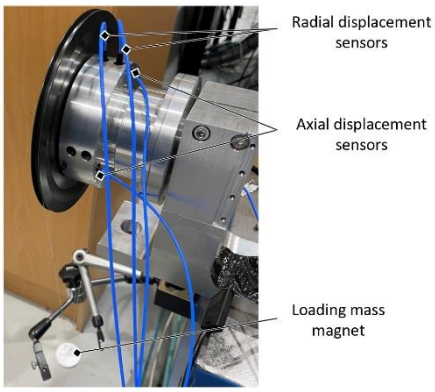

Figure 4. Radial stiffness measurement setup fitted with capacitive distance sensors for measuring the spindle hub's axial and radial displacement.

2.5. Contact event measurement of the spindle

The final spindle test involved determining if the pulley hub made contact with the aerostatic bearings under operating conditions. Because the aerostatic spindle bearings are much softer than the fibre pulley hub, it is unfavorable for the hub to make contact with the bearings while rotating. A measurement device capable of quantifying the friction moment of the spindle

was designed to aid in identifying potential contact events between the bearings and hub surfaces (Figure 5).

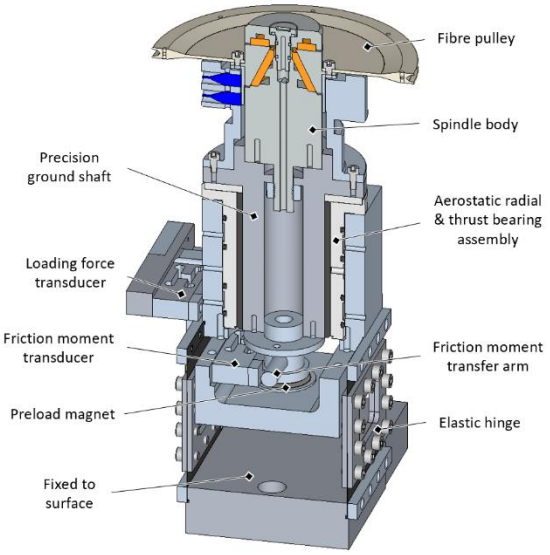

Figure 5. Cutaway view of the friction moment measurement device. The investigated spindle rests on top of a linear flexure guide and a rotational gas bearing.

2.5.1. Friction moment measurement device operating principle

The spindle body is mounted to a precision-ground shaft that rests inside an aerostatic radial and thrust bearing assembly. The shaft is preloaded against the aerostatic thrust bearing with a magnet that lies below the bearing assembly. The bearing assembly constrains the spindle body and ground shaft to only one degree of freedom: rotation around their vertical axes. This constrainment method is contactless due to the nature of aerostatic bearings. A hardened steel arm is fastened to the end of the ground shaft closest to the preload magnet. This arm interacts with a force transducer via sphere and plane contact (**Error! Reference source not found.**). If the fibre pulley hub contacts the aerostatic spindle bearings, the reaction moment will be transferred through the ground shaft causing the arm to press against the friction moment force transducer.

The aerostatic spindle was driven by another fibre pulley which was fixed in a CNC mill spindle. A 0.2 mm diameter polymer wire was the transfer mechanism between the two pulleys. The elastic hinges constrain the assembly's lateral deflection to a single axis in the horizontal plane when the spindle is loaded radially. To radially load the aerostatic spindle, the mill spindle is moved away from the friction moment measuring device until the loading force transducer reaches the desired value. In the event of significant contact between the spindle hub and spindle bearings, a sudden rise in the friction moment reading should occur. It is assumed that the spindle hub is not contacting its aerostatic bearings while rotating in an unloaded state. Figure 8 shows the spindle being driven during a test cycle. The test cycles were conducted in the following manner:

1. Supply the spindle and the friction measurement device's support bearings with 6 bar of dried, compressed air.
2. With the polymer wire around both pulleys, move the drive pulley in the loading direction until the loading transducer reads 500 ± 2 g.
3. Spin the drive pulley to 200 RPM and let the system settle for 5 seconds.
4. Record sensor data from the friction moment transducer and the loading force transducer for 30 seconds.
5. Repeat Step 2 whenever the loading transducer reads outside of the desired range and repeat Steps 3 and 4 in 200 RPM increments until a speed of 8 000 RPM is reached.

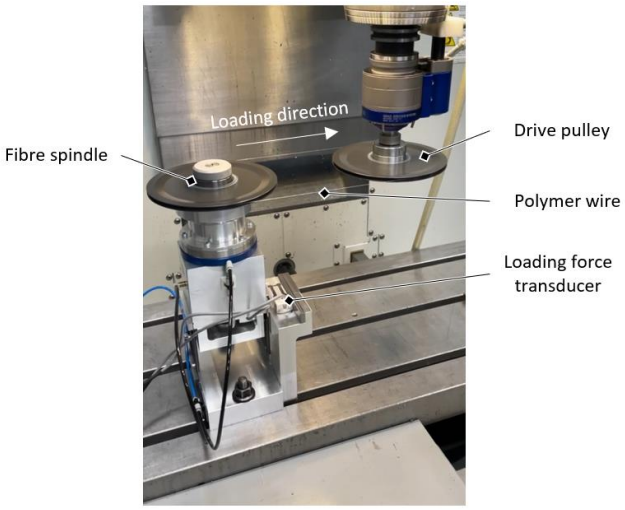

Figure 6. Friction moment measurement device in operation

3. Results and Discussion

The results of this study are presented in three sections. The first two will encompass the static loading behaviours of the capstan, and the last will show the contact event measurement results.

3.1 Static axial stiffness

The capstan's force-displacement relationship when loaded axially with calibrated masses is shown in Figure 7.

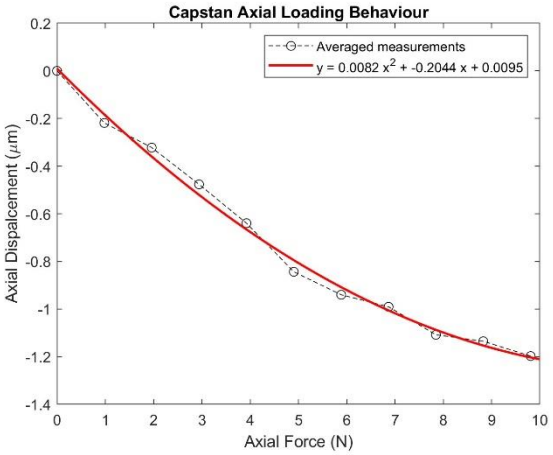

Figure 7. Axial displacement vs. force plot under static conditions.

Regarding the static performance of the aerostatic capstan, Figure 7 suggests the capstan behaves nonlinearly when loaded axially. Nonlinear spring constants are a common characteristic of porous aerostatic bearings [7]. At an axial force of 5 N, the capstan's axial stiffness is 8.5 Nμm^{-1}, and at an axial force of 10 N, 22.8 Nμm^{-1} is the resulting axial stiffness. These values were found by differentiating the curve fit line in Figure 8.

3.2 Static radial stiffness

The capstan's force-displacement relationship when radially loaded with calibrated masses is shown in Figure 8.

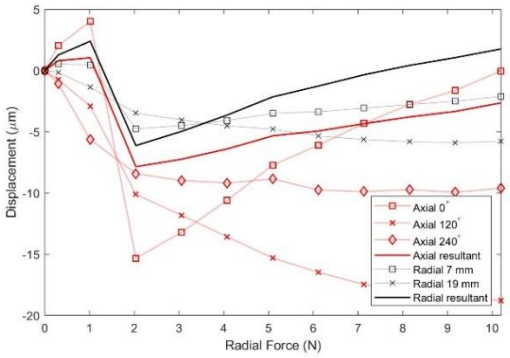

Figure 8. Radial loading displacement vs. force plot under static conditions showing the outputs of the three axial displacement sensors and the two radial displacement sensors.

Determining the capstan's static radial stiffness is less trivial than its axial stiffness due to the apparent tilting of the hub under radial load. Figure 10 suggests unpredictable displacement behavior between 0 and 2 N of radial load, however, there exists a more predictable force-displacement relationship between 2 and 10 N of radial load. The radial resultant in Figure 10 suggests a nonlinear force-displacement relationship between 2 and 10 N of radial load, with a radial stiffness of 1.1 $N\mu m^{-1}$ when loaded with 5 N and 1.4 $N\mu m^{-1}$ when loaded with 10 N. The radial resultant was found by calculating the deflection of the hub's center point using standard geometric relationships. The axial resultant was found by averaging the readings of the three axial displacement sensors. These findings suggest the capstan's design features a significantly higher axial stiffness when compared to its radial stiffness.

3.3 Contact event identification during operation

The results of the friction force test cycle are shown in Figure 9 and in Figure 10.

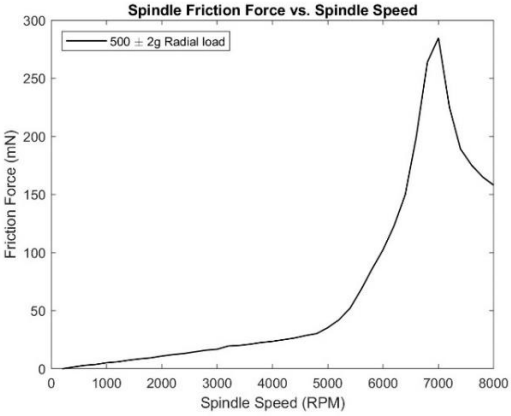

Figure 9. Friction force vs. spindle speed plot under dynamic operating conditions

The results of the friction measurement test cycle suggest the spindle hub makes contact with the graphite aerostatic bearings under dynamic operating conditions. Figure 10 shows a linear relationship between spindle speed and friction force from 200 to 4 800 RPM, suggesting no hub-bearing contact. Above 4 800 RPM, the friction force quickly rises in an exponential manner until 7 000 RPM is reached. After disassembling the capstan post-test, graphite deposits are present on the spindle hub's bearing surface indicating contact was made (Fig. 11).

Given the wide range of speed over which the friction force rises exponentially, mechanical resonance of the rotor is an unlikely cause of the sudden rise in friction. A possible cause of this instability could be due to the "air hammer" effects that can be present in aerostatic bearings that are underdamped [8]. Manufacturing errors in the spindle hub and graphite bearings could also cause an uneven air gap height across the conical bearing surface resulting in rapid changes in air gap heights during high rotational speeds.

Figure 10. Graphite deposits after contact event testing

5. Conclusions

The three measurement setups presented were successful in evaluating the fibre capstan's static and dynamic performances. The most important deliverable was the capstan's dynamic performance, but the undesirable contact-event results suggest design modifications are required to spin smoothly under the intended operating conditions. Its weaker static radial stiffness, when compared to its static axial stiffness, is most likely a cause of failure in the dynamic environment.

Possible solutions to the current design could involve increasing the spindle's radial stiffness by lowering the conical ratio of the hub and elongating the journal bearing. Replacing the annular thrust bearing with an opposing tapered journal bearing would also increase the spindle's radial load capacity while still axially constraining it. Despite the shortcomings of the presented spindle design, implementation of porous aerostatic bearings in glass fibre production equipment appears to be viable. Aerostatic bearing systems are often difficult to perfect during the first design process, therefore a re-design of the spindle would likely bring the implementation of aerostatic bearings one step closer in the glass fibre production industry.

References

[1] Li W, Liu M, Ren Y and Chen Q 2019 A high-speed precision micro spindle use for mechanical micro-machining *Int J Adv Manuf Technol* **102** 3197–3211

[2] Lu X, Paone M, Usman I, Moyls B, Smeds K, Rotherhofer G and Slocum A 2009 Rotary-axial spindles for ultra-precision machining *CIRP Annals* **58** 323-326

[3] Shimada K, Wakabayashi D, Shimoyakawa Y, Kawada S, Miyatake M and Yoshimoto S 2022 Numerical study on the rotational and machining accuracy of an end-milling process with spindles supported by aerostatic bearings *Proc. Instit. Mech. Eng. Part C: J Mechanical Engineering Science* **236** *10541-10553*

[4] Gao S, Cheng S, Ding H, Computational design and analysis of aerostatic journal bearings with application to ultra-high speed spindles 2016 *Proc. Instit. of Mech. Eng. Part C: J Mechanical Engineering Science* **231** 1205-1220

[5] Li W, Zhou Z, Xiao H and Zhang B 2015 Design and evaluation of a high-speed and precision microspindle *The Int. J. Adv. Manuf. Tech.* **78** 997-1004

[6] Yoshimoto S, Oshima S, Danbara S, Shitara T 2002 Stability of Water-Lubricated, Hydrostatic, Conical Bearings With Spiral Grooves for High-Speed Spindles *Jr. of Tribology* **124** 398-405

[7] Vainio V, Miettinen M, Majuri J, Theska R, Viitala R 2023 Manufacturing and static performance of porous aerostatic bearings *Precision Engineering* **84** 177-190

[8] Arghir M, Hassini M, Balducchi F, Gauthier R 2016 Synthesis of Experimental and Theoretical Analysis of Pneumatic Hammer Instability in an Aerostatic Bearing *J. Eng. Gas Turbines Power* **138**